Millimeter- and Submillimeter-Wave Observations of Low Vapor and Liquid Water Amounts in the Arctic Winter

D. Cimini, E.R. Westwater, M. Klein, and V. Leuski
Cooperative Institute for Research in Environmental Sciences
University of Colorado
Boulder, Colorado

D. Cimini
Istituto di Metodologie per l'Analisi Ambientale – National Research Council
Tito Scalo (PZ), Italy

E.R. Westwater, A.J. Gasiewski, M. Klein, and V. Leuski
National Oceanic and Atmospheric Administration – Physical Science Division
Boulder, Colorado

A.J. Gasieski
Center for Environmental Technology
University of Colorado
Boulder, Colorado

J.C. Lilgegren
Argonne National Laboratory
Argonne, Illinois

Introduction

Water vapor and cloud liquid measurements during cold and dry conditions are difficult because of the lack of sensitivity of conventional instruments to low amounts (Racette et al. 2005). On the other hand, millimeter (mm)- and submillimeter (submm)-wavelength radiometry may offer a powerful tool to increase the sensitivity during Arctic conditions. In response to this need, the Microwave System Development branch of National Oceanic and Atmospheric Administration Physical Science Division designed and developed a 25-channel radiometer operating in the mm- and submm-wavelength spectral region. The instrument, called the Ground-based Scanning Radiometer (GSR), was first deployed during the Arctic Winter Radiometric Experiment (March–April 2004, see Westwater et al. 2006), held at the Atmospheric Radiation Measurement (ARM) Program's North Slope of Alaska (NSA) site near Barrow, Alaska.

In the next Section, details of the GSR and other instruments operating at the ARM NSA site are given. Next, a sensitivity study is carried out to demonstrate the increased sensitivity of mm and submm-wavelength channels to small changes in water vapor and liquid contents relative to conventional microwave instrumentations. Finally, we show preliminary retrievals obtained with a linear regression technique, and we discuss the comparison with ARM operational products.

Instrumentation

The set of GSR channels includes 11 channels in the low-frequency wing of the oxygen complex at 60 GHz (50.2, 50.3, 51.76, 52.625, 53.29, 53.845, 54.4, 54.95, 55.52, 56.025, 56.215, and 56.325 GHz), 2 polarized channels at 89 GHz, 7 channels distributed near the water vapor absorption line at 183.31 GHz (183.31±0.55, ±1, ±3.05, ±4.7, ±7, ±12, ±16 GHz), 2 polarized channels at 340 GHz, and 3 channels near the strong water vapor absorption line at 380.2 GHz (380.197±4, ±9, ±17 GHz). The set of channels was selected to provide retrievals of precipitable water vapor (PWV) and cloud liquid water path (LWP), and temperature and humidity profiles. The GSR calibration procedure includes frequent (~150 ms) switching between internal loads and less frequent (2 min) observations of two external targets located in the protective housing. Moreover, the tipping curve method is applied at each scan to tune the gain (2 min) when low attenuation occurs, yielding an expected accuracy of about 1.0-1.5 K depending upon channel.

During the experiment, the GSR joined the resident instrumentation at the ARM NSA site, including the dual channel microwave radiometer (MWR, channels at 23.8 and 31.4 GHz) and a twelve-channel microwave radiometer profiler (MWRP, channels at 22.235, 23.035, 23.835, 26.235, 30.0, 51.25, 52.28, 53.85, 54.94, 56.66, 57.29, and 58.8 GHz). The spectral locations of GSR, MWR, and MWRP channels are shown in Figure 1, together with an atmospheric opacity (τ) spectrum typical of Arctic conditions. Note that the opacity for the mm and submm channels is one-two orders of magnitude larger than for the centimeter-wavelength (20-30 GHz) channels of the MWR and MWRP. Moreover, the frequency-squared dependence of liquid water absorption makes the opacity due to liquid clouds to be much larger for mm and submm channels than for lower frequency channels. This larger opacity, with the associated increased sensitivity, makes mm and submm channels appealing for the accurate retrieval of very low amounts of PWV and LWP, typical of the Arctic, at the expense of a higher degree of non-linearity.

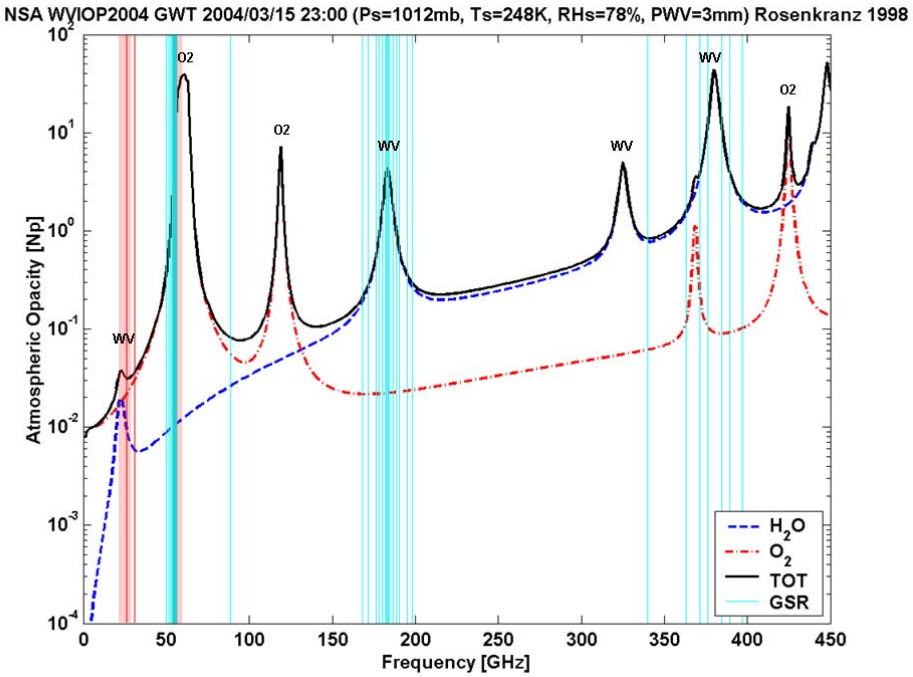

Figure 1. Atmospheric opacity for Arctic conditions. Vertical lines indicate the spectral locations of GSR (cyan) and MWR (red) channels. The red-filled boxes indicate the spectral range spanned by MWRP.

Sensitivity Study

A quantitative study of the MWR, MWRP, and GSR channel sensitivity to PWV and LWP has been carried out, following the flow chart pictured in Figure 2. As indicated in Figure 2, the calibrated (level 2.4) brightness temperatures (T_b) have been first divided in clear and cloudy conditions, according to the readings of the MWR PWV retrieval and the sky infrared temperature measured by the MWRP 10 micron channel. Once clear-sky T_bs have been selected, the relationship with PWV, as retrieved by MWR, is estimated by curve fitting. Introducing the cosmic background T_c and the mean radiative T_{mr} temperatures (Westwater 1993), we compute a 3-parameter fit (a, b, T_{mr}) by assuming an approximate relationship between T_b and PWV, i.e.,

$$T_b = T_c \cdot \exp(-\tau) + T_{mr} \cdot (1-\exp(-\tau)) \text{ with } \tau = a + b \cdot PWV \quad (1)$$

and using unconstrained nonlinear optimization (Nelder-Mead simplex method, Lagarias et al. 1998). We set the initial values of a, b, and T_{mr} to [0.0, 1.0, max(T_b)], and this choice usually leads to a convergence for all channels except for the most transparent ones (i.e., 20-90 GHz). However, for these channels the opacity is low enough that a 2-parameter linear fit, i.e.,

$$T_b = a + b \cdot PWV \quad (2)$$

and using a least-square solution is still accurate. Using the described method, we produced the sensitivity plots shown in Figure 3. Limiting the range of PWV to less than 1.5 mm, and assuming the linear relationship in (2) for all the channels, we are able to compare our results with the simulations of Racette et al. (2005) (obtained using the Rosenkranz [1998] absorption model), as shown in Table 1. For those channels that were considered in Racette et al. (2005) and available during the experiment, the agreement is good and the two estimates usually fit within the 99% confidence interval. From this table it can be seen that the sensitivities of mm and submm channels to PWV outperform the one at 20-30 GHz by a factor ranging from 1.5 to 69. The next step is to quantify the sensitivity to LWP. We select cloudy-sky T_bs according to MWR PWV and MWRP T_{ir}, and we remove the PWV contribution by using the T_b-PWV relationship we determined in the previous step (see Figure 2) and the MWR retrievals. The remaining δT_b is fitted against LWP (estimated by MWR) with a linear curve, obtaining the plot in Figure 4 and the values in Table 2 (for selected channels only). There are two things to note: first, the intercept is usually small (~0.5 K), especially for 20-90 GHz channels, which means the water vapor contribution has been removed effectively. For higher frequency channels, the intercept is larger (~2 K) although it's still modest with respect to the range of T_b variation due to PWV changes. Second, mm and submm channels show a larger sensitivity (indicated by the slope of the linear fit) with respect to 20-30 GHz, with an improvement factor from 3 to 4. Finally, the sensitivity values reported in Tables 1 and 2 demonstrate the enhanced sensitivity of mm and submm respect to conventional radiometry for measurements of low PWV and LWP contents. Of course, these conclusions are valid only for very dry conditions, as the sensitivity of mm and submm channels would fade with increasing PWV. Conversely, the sensitivity of 20-30 GHz channels remains almost invariant, making these frequencies usable in a large range of conditions.

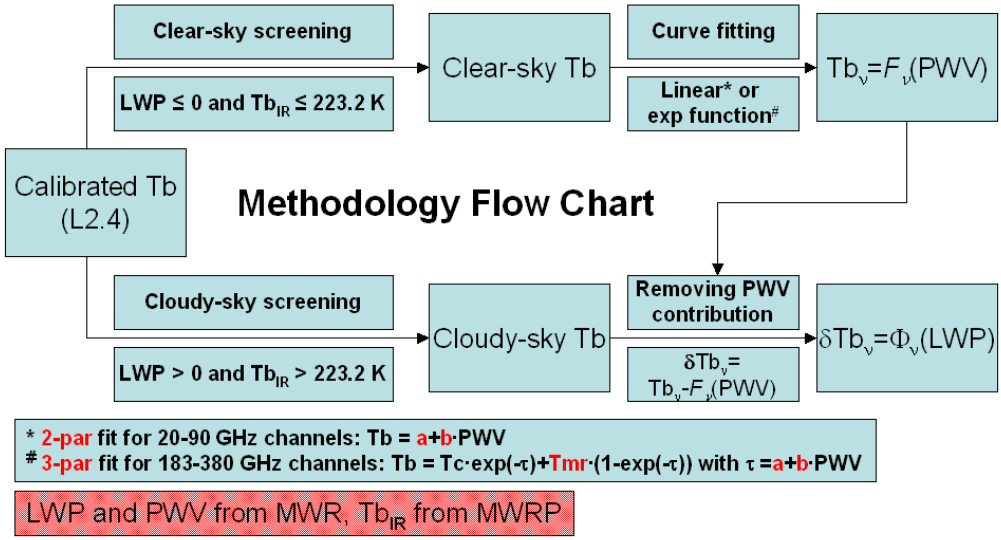

Figure 2. Methodology flow chart for the sensitivity study.

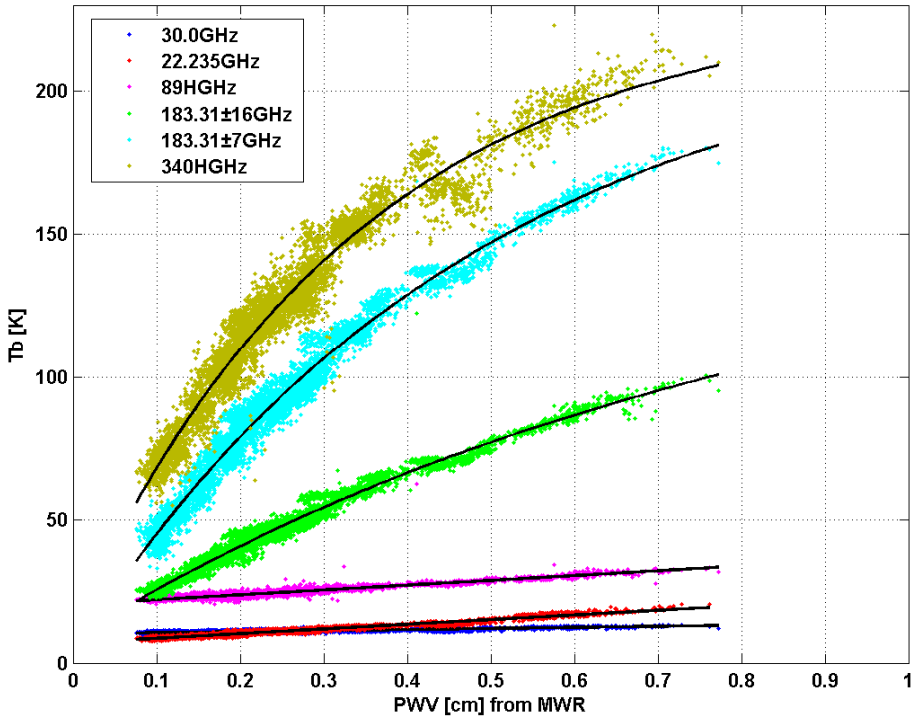

Figure 3. Measured T_b response to PWV in clear sky for selected MWRP and GSR channels.

Table 1. Simulated and measured sensitivity to PWV for selected channels. Measurements are from the Arctic Winter Radiometric Experiment (WVIOP 2004). Simulations were computed using the absorption model in [4]. CI stands for Confidence Interval.

After Racette et al. [1]		**WVIOP2004 (measured)**	
0.5<PWV<1.5 mm		**0.8<PWV<1.5 mm**	
f(GHz)	**S_{sim}(K/mm)**	**S_{meas}(K/mm)**	**99%CI(K/mm)**
23.8	1.25	1.28	0.05
31.4	0.34	0.29	0.07
89.0	1.81	1.84	0.21
150.0	6.95	NA	NA
183.3±1	78.60	87.13	3.93
183.3±3	75.00	68.04	3.04
183.3±7	39.20	31.78	1.94
183.3±16	NA	13.84	0.69
220.0	14.60	NA	NA
340.0	44.50	42.04	2.36

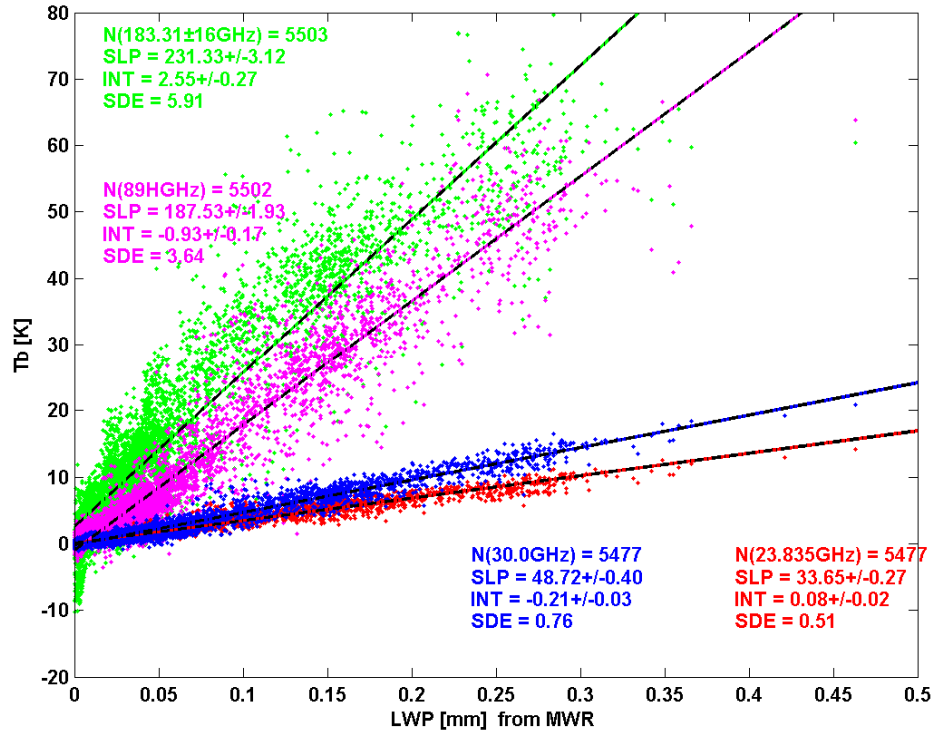

Figure 4. Measured T_b response to LWP for selected MWRP and GSR channels. The contribution of water vapor has been removed following the diagram in Figure 2. Number of elements (N), slope (SLP) and intercept (INT) of a linear fit, standard estimation error (SDE) for all four channels are also reported. SLP is in K/mm, while INT and SDE are in K. Uncertainties represent the 99% confidence interval.

Table 2. Measured sensitivity to LWP for selected channels.

F(GHz)	Slope (K/mm)	99%CI (K/mm)	Interc. (K)	99%CI (K)
22.235	28.34	0.32	0.34	0.03
23.035	32.79	0.30	0.27	0.03
23.8	32.28	0.08	0.14	0.01
23.835	33.65	0.27	0.08	0.02
26.235	39.85	0.35	-0.11	0.03
30.0	48.72	0.41	-0.21	0.03
31.4	55.61	0.08	0.14	0.01
89 H	187.53	1.93	-0.93	0.17
89 V	187.89	1.92	-0.82	0.16
183±16	231.33	3.12	2.55	0.27
183±12	195.61	3.25	2.89	0.28
183±7	95.39	4.40	1.78	0.38

Preliminary Results for Retrievals

Due to the non-linear response of mm and submm channels to atmospheric water vapor and liquid water, a non-linear retrieval technique is recommended to exploit entirely the potential of such measurements. In fact, an Optimal Estimation Method (Rodgers 2000) initialised with a first guess taken from a Numerical Weather Prediction model, also called One Dimensional-Variational Assimilation Retrieval (1D-VAR) (Hewison and Gaffard 2006, Cimini et al. 2006a), is currently being implemented. Nonetheless, a linear technique can be applied to the most transparent channels (e.g. 89, 183+/-7, 183+/-12, 183+/-16 GHz) with acceptable results. A simulation study was carried out using linear regression trained with a synthetic a priori data set generated using 559 historical clear and cloudy profiles launched at ARM NSA, processed with the absorption model described in (Liljegren et al. 2005). Using an independent set of 63 profiles processed with the same absorption model, we estimated the retrieval accuracy for a variety of channels combinations, as showed in Table 3. As expected, Table 3 indicates that a linear technique will give unacceptable results when used with opaque channels in their non-linear regime. On the other hand, as anticipated, it shows that linear regression could provide good results when used with a combination of GSR transparent channels (89, 183+/-7, 183+/-12, 183+/-16 GHz) provided that the conditions are very dry. The best results, as one would expect, are given by a combination of centimeter- and mm-wave channels, since such a combination guarantees enough sensitivity in every condition. As a first application on real data, we applied the regression coefficients computed from the simulated training set to GSR observations. An example of preliminary results is shown in Figure 5, where PWV and LWP retrievals based on GSR 89 and 183+/-7 GHz channels are compared with ARM operational products derived from MWR. As discussed in Cimini et al. (2006b), the GSR 89 GHz T_b showed a consistent bias with respect to forward model calculations. At this point, this issue is still under study, as there is lack of evidence whether this bias is due to instrumental or rather modeling error. Since the linear regression is trained with simulated data, this T_b bias would fold into the retrievals, and would require further study. In this analysis we decided to remove this bias, by simply subtracting 3.5 K from 89 GHz T_b. Overall we see a fairly good agreement, with 0.4 and 0.01 mm mean difference for PWV and LWP, respectively. The slope of the linear fit is smaller than 1 for both PWV and LWP, meaning that for high vapor or liquid contents the GSR(89, 183+/-7 GHz) tend to underestimate with respect to the MWR. This may be a residual effect of the non-linearity associated with higher frequency channels. Other than this, the comparison is satisfactory and it demonstrates the feasibility of PWV and LWP retrievals using linear regression applied to selected GSR channels. As a further comparison, in Figure 6 we show a timesseries of MWR and GSR(89, 183+/-7 GHz) retrievals. Also illustrated is PWV computed integrating the water vapor profiles measured by radiosondes launched at the ARM Great White and Duplex sites, located near the radiometers and 2.4 km away, respectively. The radiosondes launched at these two sites have been analyzed in detail (Mattioli et al. 2006) and were judged to produce unbiased PWV. It is evident from Figure 6 that when the MWR PWV departs from GSR PWV, the radiosondes tend to agree with the latter.

Table 3. Expected Accuracy for PWV and LWP Retrievals Using a Linear Regression Technique. PWV* is in mm, while LWP** in g/m^2.

PWV* rms	LWP** rms	Channels
0.375	12.67	MWR
0.290	11.83	MWRP
0.293	4.54	MWRP+GSR(89)
0.934	104.94	GSR(89, 183±1, 3, 7)
0.247	6.43	GSR(89, 183±7, 12, 16)
0.146	5.00	MWRP+GSR(89, 183±7, 12, 16)
0.827	87.60	GSR(183±1, 3, 7, 16)

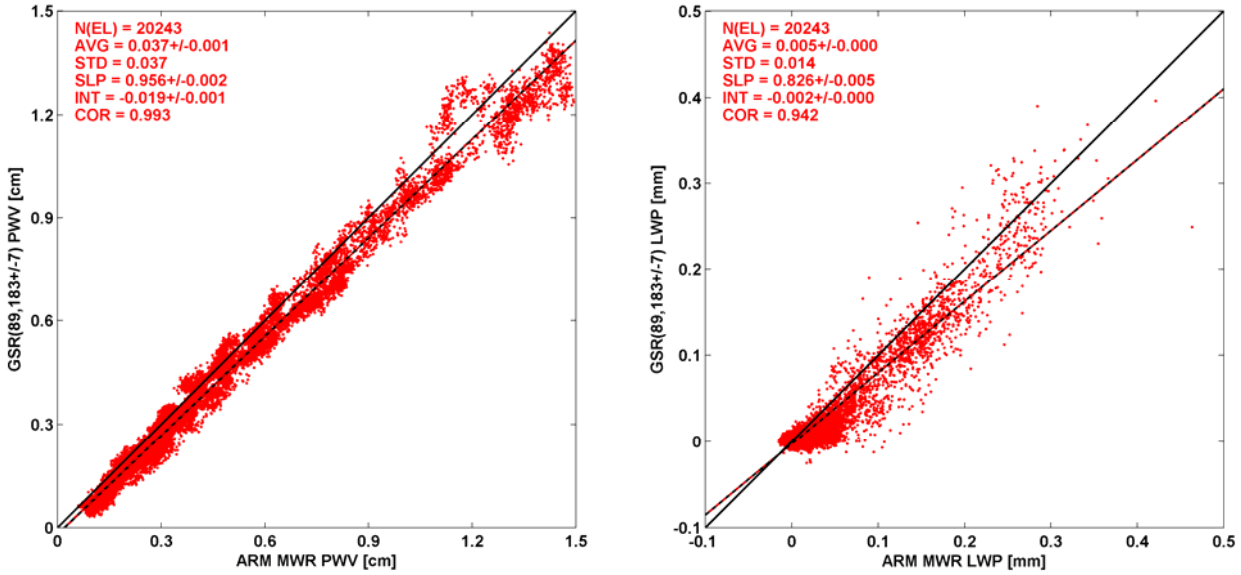

Figure 5. Comparison of PWV (left) and LWP (right) retrievals from MWR and GSR, based on 2-channel linear regression (23.8-31.4 GHz for MWR, 89-183.2±7 for GSR). Number of elements (N), mean X-Y difference (AVG), standard deviation (STD), slope (SLP) and intercept (INT) of linear fit, and correlation coefficients (COR) are also reported. Uncertainties represent the 99% confidence interval, zero meaning uncertainty is smaller than the digits shown.

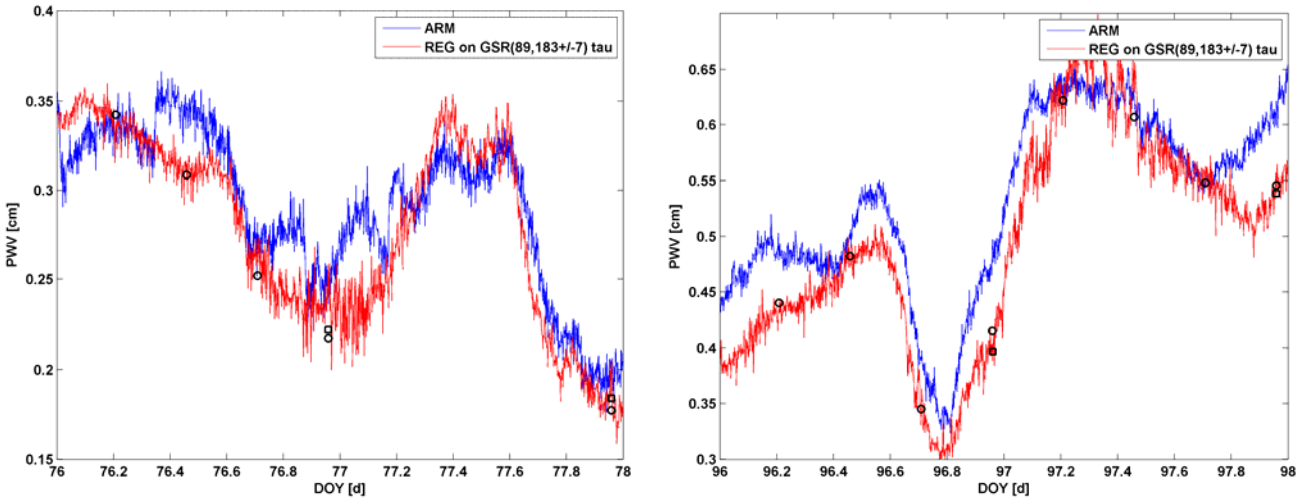

Figure 6. Time series of PWV (top) and LWP (bottom) as retrieved from MWR (blue) and GSR(89,183.2±7) (red). Black circles and squares represent PWV measured by Dyplex and Great White radiosondes, respectively. The black solid lines represent cloud detection by the MWRP infrared sensor; 0 means clear sky, while 0.05 indicates clouds overhead.

Since the launched radiosondes did not carry liquid water sensors, we do not have an independent validation for LWP. Nonetheless, by considering the infrared sky temperature measured by the MWRP, we can derive a simple cloud detection algorithm; every time the infrared temperature is higher than 223.2 K, a cloud is detected. This does not necessarily mean that there is liquid water within the cloud. On the opposite, when clear-sky is detected ($T_{ir} \leq 223.2$ K), it is likely that no liquid water is present overhead. Therefore, Figure 6 show that the ARM and GSR LWP retrieval usually follow each other and correctly detect cloud liquid when the infrared indicates cloud overpass. However, there are evident cases (as in 76.0-76.1 or 76.3-76.4 Day Of Year-[DOY]) in which the ARM operational LWP retrieval gives presence of liquid water where the GSR and the infrared sensors detect none. Although the retrieved LWP is small, approaching the uncertainty of MWR, these cases last for few hours and could be likely related to slight MWR calibration drifts. Because the sensitivity of centimeter-wave channels to low amounts of LWP is low, slight calibration drifts can be confused by the retrieval algorithm as atmospheric features. On the other hand, these results confirm the impression that mm and submm radiometry would help in these situations and thus significantly improve the retrieval of low amounts of LWP.

Conclusions and Future Work

The sensitivity of mm and submm-wavelength radiometry to low amounts of PWV and LWP typical of the Arctic conditions has been discussed and demonstrated. A quantitative study based on the data collected during the Arctic Winter Radiometric Experiment 2004 was carried out, yielding factors from 1.5 to 69 (3 to 4) for integrated water vapor (liquid water) content when compared to 20-30 GHz

radiometers. Due to the increased sensitivity, mm and submm-wavelength observations are expected to improve significantly the retrieval of PWV and LWP. An example of this feature has been given using linear regression applied to relative transparent GSR channels, which at low PWV and LWP conditions were shown to work better than retrievals based on centimeter-wavelength observations. Moreover, the use of non-linear techniques would overcome the limitations imposed by the linear regression and fully exploit the potential of mm and submm observations. Accordingly, an Optimal Estimation Method initialised with a first guess taken from a Numerical Weather Prediction model (1D-VAR) is currently being implemented as part of our ongoing research.

References

Cimini, D, TJ Hewison, L Martin, J Güldner, C Gaffard, and FS Marzano. 2006a. "Temperature and humidity profile retrievals from ground-based microwave radiometers during TUC." *Meteorologische Zeitschrift* 15(5)1-12.

Cimini, D, ER Westwater, AJ Gasiewski, M Klein, V Leusky, and S Dowlatshahi. 2006b. "The ground-based scanning radiometer: A powerful tool for study of the arctic atmosphere." submitted to *IEEE Transactions on Geoscience Remote Sensing*.

Hewison, TJ, and C Gaffard. 2006. "1D-VAR Retrieval of Temperature and Humidity Profiles from Ground-based Microwave Radiometers." In *Proceedings of the Microrad 2006*, San Juan, Puerto Rico.

Lagarias, JC, JA Reeds, MH Wright, and PE Wright. 1998. "Convergence properties of the Nelder-Mead simplex method in low dimensions." *SIAM Journal of Optimization* 9(1)112-147.

Liljegren, JC, SA Boukabara, K Cady-Pereira, and SA Clough. 2005. "The effect of the half-width of the 22-GHz water vapor line on retrievals of temperature and water vapor profiles with a twelve-channel microwave radiometer." *IEEE Transactions on Geoscience Remote Sensing* 43(5)1102-1108.

Mattioli, V, ER Westwater, D Cimini, JS Liljegren, BM Lesht, SI Gutman, and FJ Schmidlin. 2006. "Analysis of radiosonde and ground-based remotely sensed PWV data from the 2004 North Slope of Alaska arctic winter radiometric experiment." Submitted to *Journal of Atmospheric and Oceanic Technology*.

Racette, PE, ER Westwater, Y Han, A Gasiewski, M Klein, D Cimini, W Manning, E Kim, J Wang, and P Kiedron. 2005. "Measuring low amounts of precipitable water vapor using millimeter-wave radiometry." *Journal of Atmospheric and Oceanic Technology* 22:317-337.

Rodgers, CD. 2000. Inverse Methods for Atmospheric Sounding: Theory and Practice. World Scientific Publishing Co. Ltd.

Rosenkranz, PW. 1998. "Water vapor microwave continuum absorption: A comparison of measurements and models." *Radio Science* 33(4)919-928 and subsequent correction in *Radio Science*. 1999. 34(4)1025

Westwater, ER. 1993. "Ground-based Microwave Remote Sensing of Meteorological Variables." In *Atmospheric Remote Sensing by Microwave Radiometry*, J. Wiley & Sons, Inc., M. Janssen (ed.), 145-213.

Westwater, ER, D Cimini, V Mattioli, A Gasiewski, M Klein, V Leuski, and J Liljegren. 2006. "The 2004 North Slope of Alaska Arctic Winter Radiometric Experiment: Overview and Highlights." In *Proceedings of the Sixteenth Atmospheric Radiation Measurement (ARM) Program Science Team Meeting*, U.S. Department of Energy.